Journal of
Composites Science

MDPI

Article

Enhanced Dielectric and Microwave-Absorbing Properties of Poly(Lactic Acid) Composites via Ionic Liquid-Assisted Dispersion of GNP/CNT Hybrid Fillers

Ruan R. Henriques, André Schettini and Bluma G. Soares *

PEMM-COPPE, Universidade Federal do Rio de Janeiro, Rio de Janeiro 21941-594, RJ, Brazil; ruanhenriara@gmail.com (R.R.H.); alsche.schettini.20221@poli.ufrj.br (A.S.)
* Correspondence: bluma@metalmat.ufrj.br

Abstract

Poly(lactic acid) (PLA)-based nanocomposites containing a mixture of graphene nanoplatelets (GNP) and carbon nanotube (CNT) as hybrid fillers were prepared using a solution-assisted sonication process followed by melt processing. The effects of the filler dispersion on dielectric properties and microwave absorbing (MWA) performance were systematically investigated. Two ionic liquids (ILs), trihexyl-(tetra-decyl)phosphonium bis (trifluoromethanesulfonyl)imide (IL1) and 11-carboxyundecyl-triphenylphosphonium bromide (IL2), were employed as dispersing agents for the carbonaceous fillers. Incorporation of IL-treated fillers resulted in enhanced dielectric permittivity and improved MWA performance of the PLA composites. The MWA properties were evaluated in X- band and Ku-band. A minimum reflection loss (RL) of −34 dB and an effective absorption bandwidth (EAB) of 2.1 GHz were achieved for the composite containing GNP/CNT/IL2 (HB3) at a weight ratio of 2.5:0.5:0.5 wt% with one 3 mm thick layer. The superior performance of IL2 is attributed to π-π and π-cation interactions between its phenyl-containing cation and the carbonaceous fillers, as well as improved compatibility with the PLA matrix due to carboxyl groups. Additionally, three-layered composite structures, combining PLA/GNP as the outer layer with IL-assisted hybrid fillers in the core and PLA/CNT at the bottom layer, achieved an extended EAB of 4.5 GHz for GNP/HB2/CNT arrangement and 4.35 GHz for the GNP/HB3/CNT arrangement, driven by enhanced scattering and internal reflection of microwaves. These results demonstrate the potential of IL-assisted hybrid filler dispersion in PLA for developing biodegradable materials with multifunctional applications as charge storage capacitors and microwave absorbing materials for sustainable electronics.

Keywords: graphene nanoplatelets; carbon nanotube; ionic liquid; poly(lactic acid); dielectric properties; microwave absorption

Check for updates

Academic Editor: Reza Salehiyan

Received: 14 December 2025
Revised: 5 January 2026
Accepted: 7 January 2026
Published: 16 January 2026

Copyright: © 2026 by the authors. Licensee MDPI, Basel, Switzerland. This article is an open access article distributed under the terms and conditions of the Creative Commons Attribution (CC BY) license.

1. Introduction

Poly (lactic acid) (PLA) is a very popular biocompatible and biodegradable thermoplastic polyester derived from renewable resources and constitutes an important substitute of traditional fossil-based plastics in several fields [1,2]. Some of them include food packaging [3–5], and biomedical and pharmaceutical applications [6], among others. The combination of PLA with carbon-based nanomaterials gives rise to conductive polymeric composites (CPC) with superior mechanical strength, as well as electrical and thermal properties [7,8], thus expanding their field of applications, for example, as antistatic packaging for electronic devices, sensors [9], biomedical imaging and sensing [10], 3D-printed

scaffolds for tissue engineering growth [11], and electromagnetic interference shielding applications [12,13]. In this context, PLA-based CPCs containing carbonaceous fillers, such as carbon nanotube (CNT), graphene, and their derivatives have attracted increased interest due to the possibility of producing light-weight, easily processable and scalable materials that combine the biodegradability of the matrix and the electric/dielectric properties of the conductive filler. Among several carbon-based materials, graphene nanoplatelets (GNP) and expanded graphite (EG) have emerged as promising conductive filler due to their commercial availability and relatively low cost compared with other carbon-based nanomaterials [14,15]. In addition, GNP nanoparticles exhibit outstanding electrical conductivity and mechanical properties, which depend on their structural quality, number of graphene layers, etc. [16]. Numerous studies have reported significant enhancement in the mechanical performance, particularly stiffness, and modulus and tensile strength, as well as thermal stability of PLA composites, achieved through the incorporation of small amounts of GNP or their derivatives [17]. In general, GNP loadings as low as 0.25–0.50 wt% are sufficient to induce a positive reinforcement effect in PLA-based composites [18,19]. The presence of GNP also improved the thermal stability of the corresponding PLA nanocomposites [20,21].

PLA-based CPCs incorporating GNP and GNP/CNT hybrid fillers have also been extensively investigated for applications as electromagnetic interference (EMI) shielding and microwave absorbing (MWA) materials. This research area has gained increasing attention due to the growing concerns over invisible electromagnetic (EM) pollution arising from the widespread use of advanced electronic devices and wireless communication systems, which can adversely affect both human health and the performance of nearby electronic equipment [22]. Furthermore, the rapid obsolescence of electronic devices driven by the continuous technological advancements has led to a great accumulation of electronic waste. Consequently, the development of environmentally friendly conductive polymer composites for electronic applications, commonly referred as "green electronics", has become a topic of significant scientific and industrial interest. Studies related with PLA composites loaded with GNP and the GNP/CNT hybrid fillers are reported in the literature. Jalali et al. [23] prepared composites based on PLA and 10 wt% graphene nanoribbons using the solution casting technique, and reported electromagnetic interference shielding effectiveness (EMI SE) values of approximately 15 dB in both X- (8–12 GHz) and Ku- (12–18 GHz) band frequency range. A similar processing methodology and system were used by Bregman et al. [24], who reported an overall EMI SE of 12 dB at 8 GHz for PLA/GNP system with 5 wt% GNP. The melt mixing procedure was employed by Kashi et al. [25,26] and Al Saleh et al. [27,28] to develop PLA/GNP composites for EMI shielding applications. However, high amounts of GNP were usually required for achieving EMI SE higher than 10 dB, established as a standard for most EMI shielding applications. This drawback is attributed to the difficulty of GNP in dispersing within a polymeric matrix because of their great tendency for agglomeration and restacking caused by the strong van der Waals interactions between the lamellae. The use of GNP/CNT hybrid filler has been reported to enhance the electrical conductivity and EMI SE of the corresponding composites, which was attributed to the ability of CNT in acting as a bridge between the GNP platelets, resulting in the formation of the physical 3D structure [29–32]. Despite the outstanding electrical performance displayed by the CPC containing GNP/CNT hybrid filler, their use in biodegradable composites is scarce. Shi et al. [33,34] reported PLA/GNP/CNT composites with improved EMI SE by dispersing the fillers and PLA in water followed by extrusion of the filtered system into filaments for 3D-printed cellular matrices. Al Saleh et al. [28] studied the effect of GNP/CNT (1:1 by mass) in PLA matrix on EMI SE of the corresponding composite. The use of 3 wt% of GNP resulted in an overall EMI SE of 2 dB, whereas the presence of GNP/CNT (1.5:1.5 wt%) increase the EMI SE to 20 dB.

Ionic liquids were recently shown to be excellent additives for improving the dispersion of carbon-based fillers in polymeric matrices, resulting in enhanced electrical conductivity and EMI SE [35–38]. In fact, the conductivity and EMI SE were enhanced by using appropriate ionic liquids as dispersing agent for CNT in polypropylene/EVA [39], and PLA/ethylene-co-vinyl acetate (EVA) copolymers [40]. Polymerized based imidazolium ionic liquid was also successfully used to disperse CNT in PLA/polycaprolactone (PCL) blends, resulting in increased conductivity and EMI SE [41].

The EMI shielding materials interact with the EM radiation by reflection and absorption mechanisms. The reflection is governed by the interaction of the EM radiation with mobile electron carriers and is dominant in conductive materials. The absorption mechanism occurs due to the interaction of EM radiation with electrical and magnetic dipoles [42,43]. As the present work involves only dielectric particles, the influence of the magnetic absorption is irrelevant. In many applications, absorbing materials are strongly desirable to avoid self-emission of the radiation causing a secondary EM pollution. In addition, they are strategically important for defense to reduce the radar detectability [44,45]. The absorbing properties are measured in terms of reflection loss (RL). A good microwave absorbing material must present minimum RL values as low as possible and RL lower than −10 dB (corresponding to more than 90% of EM absorption) in a large frequency range, that is, a large value of specific absorbing bandwidth (EAB). Some researchers reported the microwave absorptivity in terms of reflection loss (RL) of PLA-based composites using GNP or hybrids. Kashi et al. [46] achieved RL of −49.87 dB (with thickness of 11.2 mm) by melt-blending PLA with 6 wt% GNP. Wang et al. [13] prepared PLA/GNP composite by solution mixing and compression-molding, and reported RL value of −19.5 dB at around 13 GHz with 8 wt% GNP and a sample thickness of 1.5 mm. Anjos et al. [47] prepared PLA/poly(3-hydroxybutyrate-co-3-hydroxyvalerate) (PLA/PHBV = 80:20 wt%) containing GNP, CNT, and the hybrids by melt-blending. They obtained minimum RL lower than −10 dB (corresponding to electromagnetic attenuation or electromagnetic absorption higher than 90%) only with the CNT/GNP hybrid with a specific composition and thickness.

Building upon these insights, the motivation and novelty of this work was to use ionic liquids as dispersing agents for the CNT/GNP hybrid fillers and investigate the dielectric properties at a low frequency range and microwave absorbing properties of the corresponding PLA-based composites in both the X- and Ku-band frequency range. Monolayer and multi-layer structures were investigated. The later arrangement favors the absorptivity at a larger frequency range due to the effect of multi-reflection and scattering of the radiation through several interfaces within the sample, which contribute for an efficient attenuation of the EM radiation by absorption [48–50]. Trihexyl-(tetradecyl) phosphonium bis triflimide (IL1) and 11-carboxyundecyl-triphenyl phosphonium bromide (IL2) were the ionic liquids of choice. The first one (IL1) was selected due to the enhancement of the electrical conductivity and EMI SE achieved with the addition of 5 wt% of this IL in PLA/PP composites [39]. According to previous work, these results were caused by the improved dispersion of CNT within the polymer matrix imparted by IL [39]. Regarding the second IL, the presence of carboxyl group in its structure may facilitate the interaction with PLA matrix. Some works in the literature used carboxyl-containing IL to improve the compatibility of PLA-based blends [51,52]. In addition, the presence of the three phenyl rings in the cation structure may facilitate the interaction with the graphene nanoplatelets through π-π interactions.

Despite numerous studies on biodegradable conductive polymer composites (CPCs) containing CNT and GNP, the incorporation of GNP/CNT hybrid fillers modified with ILs into a PLA matrix for enhancing microwave absorbing properties has not yet been

reported, to the best of the authors' knowledge. These findings demonstrate that combining PLA with IL-modified hybrid nanocarbon fillers not only advances the sustainability of microwave absorbing (MWA) materials but also enables scalable, lightweight, and design-flexible applications. The present study aims to minimize the required filler loading while maintaining competitive microwave absorption performance, thereby reducing materials consumption and cost, and providing deeper insight into the interfacial effects governing electromagnetic attenuation in bio-based, biodegradable composites.

2. Materials and Methods

2.1. Materials

Poly(lactic acid) (Ingeo Biopolymer 4043D) in the pellet form (density = 1.24 g cm^{-3}; melt flow rate = 6 g 10 min^{-1} at 210 °C/2.16 kg), was purchased from NatureWorks LLC (Plymouth, MN, USA). Graphene nanoplatelet (GNP) (commercial name = Graphene C750® Grade M; surface area = 750 m^2 g^{-1}; density = 2.05 g cm^{-3}) was purchased from Sigma-Aldrich, Brazil. Multi-walled carbon nanotube (CNT) (trade name = NC7000™; average diameter = 9.5 nm; average length = 1.5 µm; carbon purity = 90%; surface area = 250–300 m^2 g^{-1}; density = 1.75 g cm^{-3}; electrical conductivity = 10^6 S/m) was purchased from Nanocyl S.A. Trihexyl-(tetradecyl) phosphonium bis triflimide (IL1) (trade name = CYPHOS 109) were kindly supplied by Cytec Inc. (Woodland Park, NJ, USA). 11-carboxyundecyltriphenylphosphonium bromide (IL2) was synthesized through the reaction of 11-undecanoic acid and triphenyl phosphine (Sigma-Aldrich do Brasil; São Paulo, Brazil) according to the literature [53]. The IL2 (yield = 88–92%; melting point = 8.9 °C) is liquid was also characterized by 13C NMR analysis, whose spectrum coincides with that previously published [53]. The structure of ionic liquids is illustrated in Figure 1.

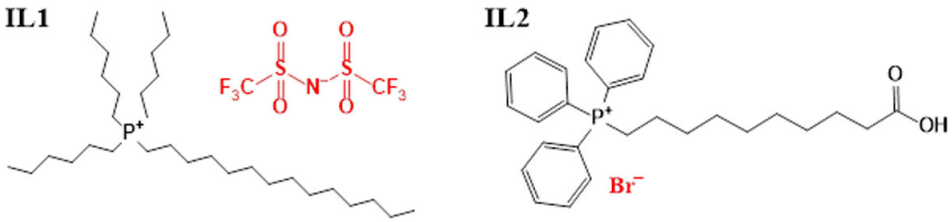


Figure 1. Chemical structures of the ionic liquids.

2.2. Composites Preparation

PLA, GNP, CNT, and the ionic liquids were dried overnight at 60 °C under vacuum to remove residual moisture. Initially, a masterbatch involving PLA and the fillers were prepared by first dissolving 6 g PLA in 100 mL tetrahydrofuran (THF) at 80 °C. Separately, a dispersion containing the fillers with or without the IL in THF was prepared using sonication in an ice bath for 15 min at 30% amplitude, using pulse mode (20 s on/10 s off). Then, the PLA solution and the dispersion were mixed and submitted to an additional sonication process for 5 min, followed by mechanical mixing using a T-25 digital Ultra-turrax from IKA Brasil, Campinas, Brazil., at 15,000 rpm. The masterbatch was dried at 60 °C, under reduced pressure for 24 h to completely remove THF. This previous treatment was performed to improve the dispersion of the fillers.

The final composites were prepared by melt-blending the master batch previously prepared with additional amount of PLA to reach the composition as indicated in Table 1. The process was performed in a Xplore MC15 HT conical twin-screw micro extruder (Xplore Instruments BV, Sittard, The Netherlands) with co-rotating screws and an internal volume of 15 mL. The blends were processed at 170 °C and 170 rpm for 4 min with the extruder in a

closed configuration. The specimens for all testing were prepared by compression-molding at 170 °C and 4 MPa for 4 min and immediately cooled down at the same pressure.

Table 1. Composition of the samples.

Sample	PLA (wt%)	GNP (wt%)	CNT (wt%)	IL (wt%)
PLA/GNP	97	3	-	-
PLA/CNT	99.5	-	0.5	-
PLA/HB1	97	2.5	0.5	-
PLA/HB2	96.5	2.5	0.5	0.5 wt% of IL1
PLA/HB3	96.5	2.5	0.5	0.5 wt% of IL2

2.3. Characterization

The rheological properties of the composites were evaluated at 180 °C on a Discovery DHR1 rheometer (TA Instrument, Inc., New Castle, DE, USA) with parallel plates geometry (25 mm diameter) and gap of 1.0 mm. The analysis was carried out under oscillatory mode, with a frequency sweep from 0.1 to 100 Hz and 0.1% strain. The X-ray diffraction (XRD) patterns were obtained on a Rigaku Ultima IV diffractometer, using a continuous scanning mode in the range of 2θ from 5° to 60°, with a step size of 0.05° s^{-1}, using the Cu-kα radiation at 40 kV and 40 mA. Dynamic mechanical analysis (DMA) was performed on a DMA Q800 from TA Instruments Inc., at a fixed frequency of 1 Hz, and a heating rate of 3 °C/min. The test was performed in a single cantilever clamp, and 0.1% deformation. AC electrical conductivity was measured on a VersaSTAT 3 potentiostat (Ametek Scientific Instruments, Berwyn, PA, USA) and a circular sample holder. The conductivity was analyzed from 10^{-2} to 10^{5} Hz at 0.1 V. The samples were compression molded into disks with 25 mm diameter and 1 m thickness and covered with a thin layer of gold (around 60 μm) to improve the contact with the electrodes.

The electromagnetic properties in the X-band (8.2–12.4 GHz) and Ku-band (12–18 GHz) frequency range were measured using an Agilent Technologies PNA-L N5231A vector network analyzer (VNA) from Keysight Technologies (Santa Rosa, CA, USA). The coaxial cables attached to Port 1 and Port 2 of the VNA equipment were connected to rectangular waveguides with cross-sections of 22.1 × 10.0 mm (for X-band) and 15.8 × 7.9 mm (for Ku-band). The samples were molded at 170 °C for 4 min to dimensions corresponding to the waveguides with a thickness of 3 mm. The reflection loss (RL) is defined as the logarithmic ratio between the reflected electromagnetic wave intensity (Er) and the incident wave intensity (Ei), as described by Equation (1), which represents the theoretical definition of RL based on electromagnetic wave amplitudes. In the experimental setup, RL was evaluated using a metal-backed configuration, in which the sample was placed on a metallic plate acting as a perfect reflector, ensuring that all transmitted radiation was suppressed. Under this condition, the reflection loss can be experimentally determined from the scattering parameter S_{11} measured by the vector network analyzer, as expressed in Equation (2):

$$Reflection\ loss\ (RL) = 10 \times \left|\frac{E_R}{E_i}\right|^2 \quad (1)$$

$$RL\ (\mathrm{dB}) = 20 \times \log|S_{11}| \quad (2)$$

3. Results

3.1. Rheological Characterization

The torque profiles as a function of the residence time during processing of the PLA-based composites are illustrated in Figure 2. All samples exhibited an initial decrease in

torque with increasing residence time, due to the melting of PLA, followed by a plateau after approximately 1 mm, indicating mixture homogeneization. At this time, the torque value of the composite containing 3 wt% GNP was quite similar to that of the composite with 0.5 wt% CNT. After this time, the torque related to the PLA/GNP sample continued to decrease whereas the torque values of the other samples stayed more stable. In contrast, the PLA/CNTcomposite exhibited higher torque values despite the lower filler content, possibly due to the 1D morphology of the nanotubes which favor the dispersion of the filler and the formation of a physical network in higher extent. The hybrid composite containing 2.5 wt% GNP and 0.5 wt% CNT presented the highest torque among all samples, which may be related to a gel-like structure formed by the synergistic interaction of the two nanostructures. Finally, the addition of ionic liquids to the hybrid systems led to a reduction in torque, likely due to the plasticizing and lubricating effects of the ILs, which promote easier flow during processing. Both ionic liquids exerted a similar influence on the flow behavior during processing, suggesting that this effect was independent of their chemical nature.

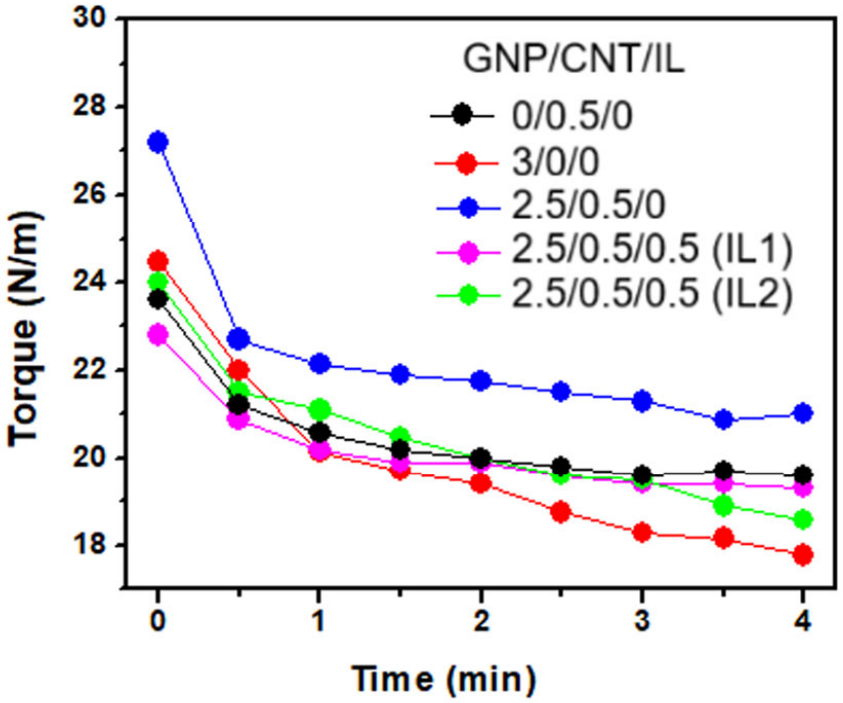


Figure 2. Torque profile during melt-processing of PLA-based composites at 170 °C and 170 rpm for 4 min.

The rheological behavior of the composites obtained by oscillatory shear measurements provides a better insight regarding the filler–matrix interactions. Figure 3 presents the complex viscosity (η*) and storage (G′) modulus as functions of angular frequency and phase angle as a function of the storage modulus (the van Gurp–Palmen plots). A summary of the rheological data extracted from these analyses is presented in Table 2. The data confirm the trends observed in torque analysis. The PLA/GNP (3 wt%) composite exhibited the lowest viscosity across the studied frequency range, supporting the hypothesis of a lubricating effect induced by the graphene nanoplatelets. Conversely, the hybrid composite containing 2.5 wt% GNP and 0.5 wt% CNT displayed the highest complex viscosity, reinforcing the evidence of a more structured network that hinders flow. According to the literature, the CNTs can act as bridges between the graphene platelets, inhibiting their aggregation and stacking [54]. The addition of ionic liquids led to a reduction in viscosity, consistent with their known plasticizing and lubricating effects. Nevertheless,

the η* profiles related to the samples with the fillers modified with IL (PLA/HB2 and PLA/HB3) are quite similar indicating that the nature of the ILs did not exert significant influence on the rheological properties.

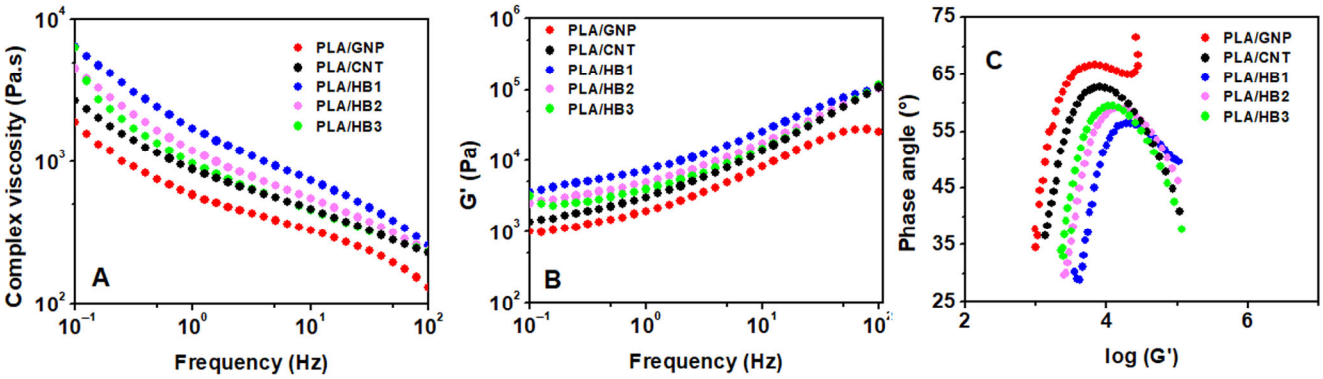


Figure 3. (**A**) Complex viscosity, and (**B**) Storage modulus as functions of frequency, and (**C**) van Gurp–Palmen plots (phase angle, δ versus storage modulus, G′) for the PLA-based composites. Measurements were perfomed at 180 °C with a frequency sweep from 0.1 to 100 Hz and 0.1% strain.

Table 2. Main rheological data related to the PLA-based composites, obtained at 180 °C with a frequency sweep from 0.1 to 100 Hz and 0.1% strain.

Sample	GNP (wt%)	CNT (wt%)	IL (wt%)	η* (0.12 Hz) (Pa.s)	G′ (0.12 Hz) (Pa)	G′x G″ (Hz)	Maximum Phase Angle (°)
PLA/GNP	3	-	-	1590	980	0.25	72
PLA/CNT	-	0.5	-	2300	1400	0.21	63
PLA/HB1	2.5	0.5	-	5500	3800	0.84	56
PLA/HB2	2.5	0.5	0.5 wt% of IL1	3970	2600	0.65	59
PLA/HB3	2.5	0.5	0.5 wt% of IL2	3860	2300	0.64	59

The storage (G′) and loss (G″) moduli data provide further insight into the internal structure of the composites. The PLA/CNT and hybrid samples exhibited an apparent plateau in the low-frequency region of the G′ curve, characteristic of the formation of a percolated nanostructured network. Figure S1 in the Supporting Information exhibits the G′ and G″ plots against the frequency. All composites displayed G′ > G″ at a very low frequency, indicating a solid-like viscoelastic behavior, which is typical of structured filler inside the polymer matrix.

To further elucidate these structural differences, van Gurp–Palmen plots (phase angle δ versus storage modulus G′) were constructed, as indicated in Figure 3C [55]. δ values approaching 90° at low G* indicates a dominant viscous state [56]. The deviation from 90° suggests that the solid-like state starts to be important. In this context, the sample containing HB1 presented a higher deviation than the binary composites indicating the formation of physical networks in higher extent, as also observed from η* behavior.

3.2. Dynamic-Mechanical Analysis of PLA Composites

The dynamic-mechanical analysis (DMA) of the PLA-based nanocomposites is shown in Figure 4, in terms of storage modulus and tan delta against temperature. Table 3 summarizes the main DMA data corresponding to the PLA and the composites. The glass transition temperature was taken at the maximum of the tan delta peak. The neat

PLA sample exhibited the lowest values among all systems, with a storage modulus of 1400 MPa at 30 °C and a glass transition temperature (Tg) of 69 °C. After the glass transition temperature, the E′ value increased due to the cold crystallization, which is typical of PLA samples due to its low crystallization rate [57]. The temperature where the E′ started to increase was set as 76 °C. The addition of 0.5 wt% of CNT resulted in a significant increase in modulus, indicating a reinforcing effect of the filler, even in a low amount. The composite containing 3 wt.% GNP exhibited an additional improvement on storage modulus in the glassy region (E′ = 2280 MPa at 30 °C) and the highest Tg (74.0 °C). This behavior can be attributed to the reinforcing effect of graphene, which, when well dispersed within the PLA matrix, enhances load transfer efficiency, and restricts chain mobility.

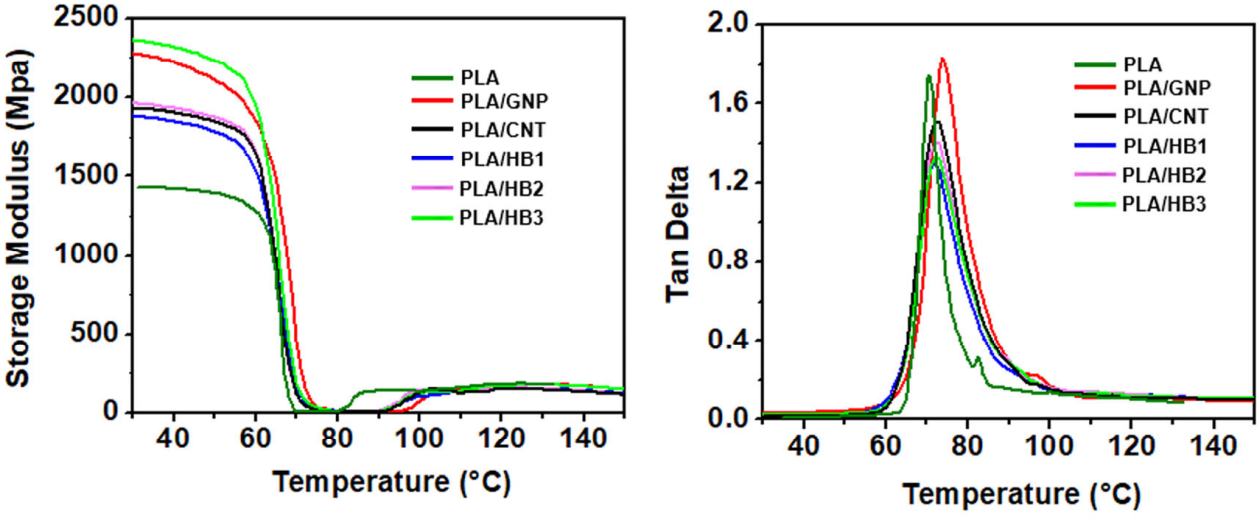


Figure 4. Dynamic-mechanical analysis versus temperature of PLA and their composites (conditions: frequency = 1 Hz; deformation = 0.1%; heating rate of 3 °C/min).

Table 3. Main dynamic-mechanical data related to the PLA-based composites.

Sample	GNP (wt%)	CNT (wt%)	IL (wt%)	E′ at 30 °C (MPa)	Tg (°C)	T_{cc} (°C)
PLA	-	-	-	1400	69	76
PLA/GNP	3	-	-	2280	74	89
PLA/CNT	-	0.5	-	1930	72	85
PLA/HB1	2.5	0.5	-	1880	72	85
PLA/HB2	2.5	0.5	0.5 wt% of IL1	1960	72	83
PLA/HB3	2.5	0.5	0.5 wt% of IL2	2360	72	85

The hybrid system without ionic liquids (2.5/0.5) displayed an E′ value lower than the composites containing CNT (0.5 wt%) or GNP (3.0 wt%), suggesting that the hybridization alters the reinforcing mechanism of GNP, possibly due to changes in dispersion and filler–filler interactions. However, the incorporation of ILs modified this trend. The system modified with the IL1 displayed a slight improvement of E′, when compared with the composite containing non-modified GNPCNT hybrid filler. On the other hand, the composite loaded with GNP/CNT/IL2 hybrid demonstrated a remarkable improvement in the glassy storage modulus (E′ = 2360 MPa at 30 °C). These results suggest that the carboxyl group in the IL2 contributes to the filler–matrix compatibility, promoting stronger interfacial interactions and a more efficient stress transfer. The Tg values of PLA/CNT and the hybrids displayed a slight increase when compared to the neat PLA.

All composites exhibited higher cold crystallization temperature, indicating that the presence of filler delayed the crystallization process. Generally, the carbonaceus fillers exert

a nucleating effect on the PLA chain, thus decreasing the T_{cc} values. However, according to the literature, the filler can restrict the mobility of the molecular chain segment, thus difficulting the polymer chain to align into a crystalline structure [58].

3.3. Electrical and Dielectric Properties

The AC conductivity versus frequency for the PLA-based composites is illustrated in Figure 5. The samples containing 3 wt% GNP displayed a typical insulating behavior, characterized by a nearly linear dependence of conductivity with frequency and the absence of a low frequency plateau. The PLA/CNT composite displayed a discrete increase in conductivity at low frequency, but a strong dependence of the conductivity with frequency. These results indicate that, at these concentrations, no continuous conductive network was formed. In contrast, the composite containing GNP/CNT (2.5:0.5 wt%) hybrid exhibited a remarkable enhancement in conductivity at low frequency range (3×10^{-7} S/m), spanning up to around two orders of magnitude compared with the single-filler systems. This value is significantly higher than the electrical conductivity of PLA/CNT (0.5 wt%) and PLA/GNP (3.0 wt%), indicating a significant synergistic effect, as reported in the literature [28,59,60]. This result is attributed to the mutual action of one filler to the other, whereas GNP contributes to a de-agglomeration of the CNT bundles, the CNTs act as 1D bridges that interconnect adjacent graphene sheets. This configuration reduces the interparticle distance and facilitates the formation of continuous conductive pathways, effectively lowering the percolation threshold.

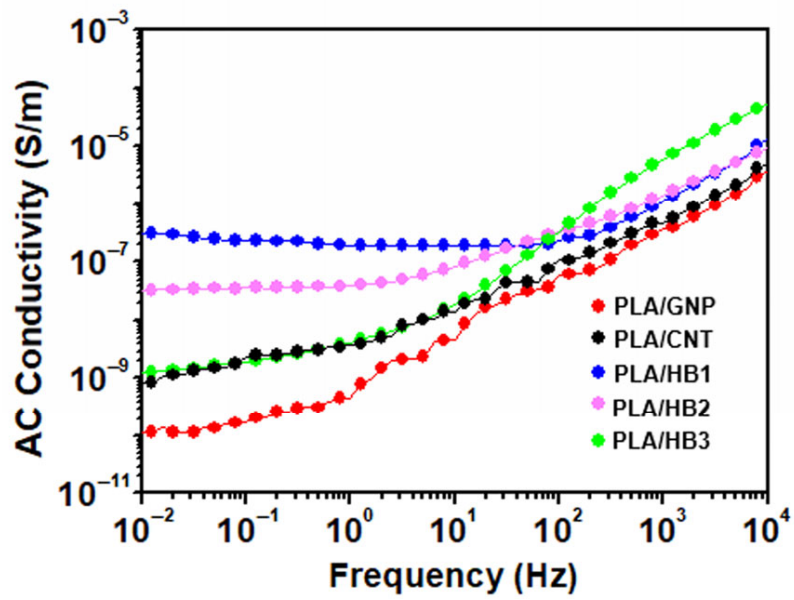


Figure 5. AC electrical conductivity as a function of the frequency for PLA-based composites.

The functionalization of the filler with ILs decreased the conductivity. This behavior may be attributed to the better dispersion of the filler (CNT and/or GNP) within the PLA matrix, with the formation of insulating layer that limits the electron movements and avoids contact between the conductive particles, as observed in other studies [61–63]. This hypothesis can be confirmed by dielectric properties.

Figure 6 illustrates the dielectric permittivity (ε'), dielectric loss (ε''), and dielectric tangent as a function of the frequency. The permittivity decreases exponentially with an increase in the frequency at a low frequency region. At a low frequency range, the significant increase in permittivity is ascribed to the Maxwell–Wagner–Sillars (MWS) polarization, also known as interfacial polarization, which occurs due to the accumulation of charge carriers at the interface between two materials [61,64]. The presence of IL in the hybrid

fillers resulted in a substantial increase in the dielectric constant at a low frequency range, indicating a higher MWS effect due to the entrapment of the charge carriers in the interface region between the filler/IL and the PLA matrix. This feature confirms the ability of ILs in interacting with the carbonaceous filler surface. The non-conducting nature of the IL segments helps to form a dielectric and insulating thin layer which prevents the direct contact of the conducting fillers and the formation of the conducting pathway. The composite with GNP/CNT/IL1 (PLA/HB2) presented the highest ε' value at low frequency. However, the GNP/CNT/IL2 (PLA/HB3) displayed the lowest loss tangent, which explains the lower conductivity when compared with the other hybrids. The loss values of these systems are lower than the permittivity, which is very important for applications, as charge storage capacitors and electromagnetic wave absorption materials [61,65]. The success of the ionic liquid in improving the dielectric properties of the PLA composites is due to the good dispersion of the CNT and GNP by the IL with the formation of many microcapacitors inside the PLA matrix, consisted of a thin insulating layer of IL surrounding the conductive particles.

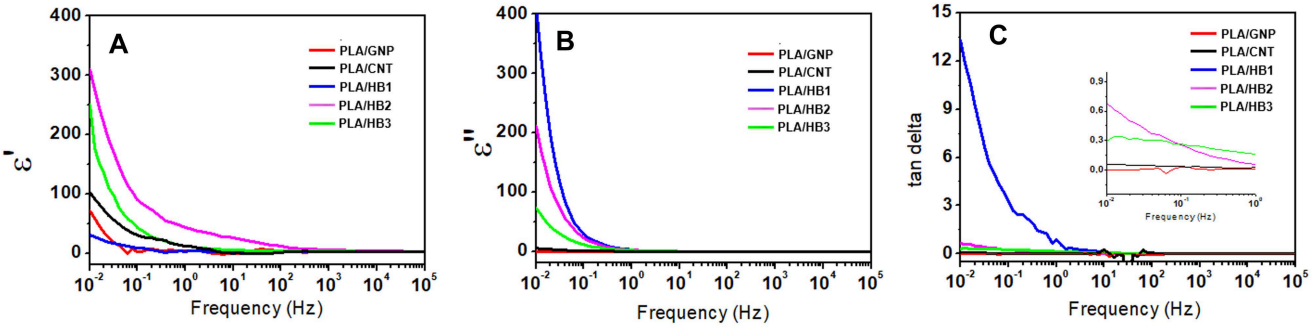


Figure 6. Frequency dependence of (**A**) electrical permittivity,(**B**) dielectric loss, and (**C**) tan delta of PLA-based nanocomposites.

The PLA composite containing GNP/CNT (2.5:0.5 wt%) without IL lead to a very high dielectric loss compared to the permittivity values, due to its higher conductivity which imparts large leakage current, originated from the direct contact between conductive fillers.

3.4. Microwave Absorbing Properties of Monolayer Structure

As it was mentioned in the Introduction, materials that can attenuate the EM radiation by the absorption mechanism are of great interest to avoid the secondary pollution caused by the reflected radiation and also for military applications to protect the target against radar detectability. Therefore, in this topic, the effect of the hybrid filler and the presence of ionic liquids on the microwave absorbing properties of PLA nanocomposites are discussed in detail. The EM attenuation by absorption is described in terms of reflection loss (RL) and can be measured directly from the scattering parameters obtained in the VNA equipment, using Equation (2). A good microwave absorbing material should present an impedance as close to the air as possible to make possible the penetration of the radiation inside the material without reflection at the surface. Then, the dielectric particles in the material interact with the radiation, causing multi-reflection and scattering thus contributing for its dissipation.

Figure 7 displays the measured RL curves in the X- and Ku-band frequency range. The PLA/GNP (3 wt%) composite presented a better response than that containing CNT (0.5 wt%) despite the latter presenting an electrical conductivity one order of magnitude higher. This behavior indicates that microwave absorption is not governed solely by electrical conductivity but also by impedance matching and dielectric loss mechanisms. In fact, a minimum RL of −13 dB at 13.95 GHz corresponding to an EM attenuation of

around 95% was obtained for the PLA/GNP system. This outstanding observed response may be attributed to the presence of many interfaces and the planar geometry of this filler that increase the interfacial polarization and favor the multi-reflection and scattering of the radiation and, consequently, the attenuation of the radiation.

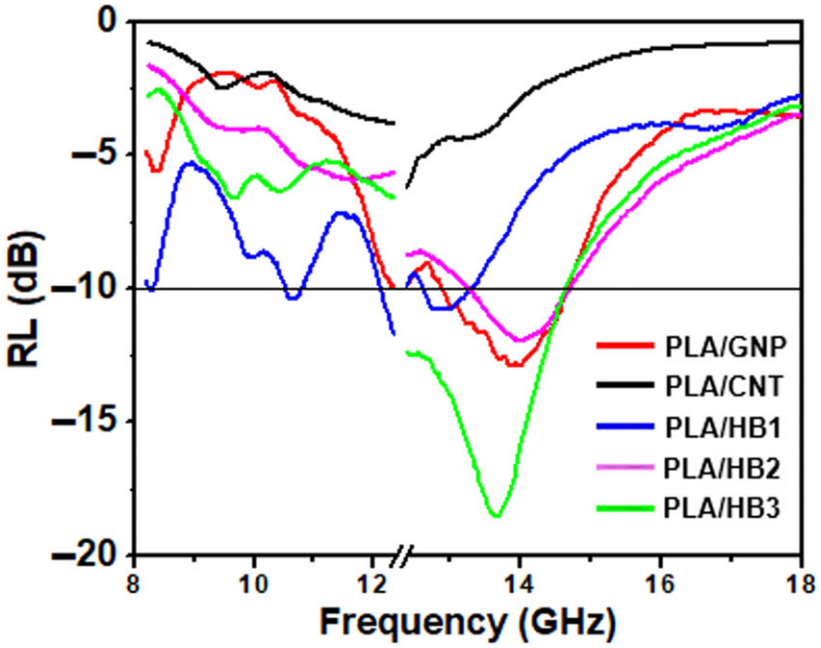


Figure 7. Measured RL values in the X- and Ku-band frequency range for the PLA nanocomposites (samples with 3 mm thickness).

The system containing IL2 (PLA/HB3) presented outstanding absorbing properties in the Ku-band, with minimum RL of −18.5 dB (around 98.5% of EM radiation) and a EAB of 2.28 GHz. This behavior should be due to the low conductivity associated with the high dielectric constant combined with very low dielectric loss, which increase the interfacial polarization. The decrease in EM attenuation of the system containing IL1 may be due to its higher conductivity compared with the system containing IL2, thus contributing to the increase in impedance mismatching.

The absorbing properties of a material are primarily governed by the dielectric and magnetic properties as well as conductivity and impedance matching. The complex permittivity ($\varepsilon^* = \varepsilon' - j\varepsilon''$) of the composites is an important parameter for understanding their shielding performance. The real part (ε') is generally associated with energy storage, while the imaginary part (ε'') is linked to energy dissipation. Figure 8 presents the frequency-dependent evolution of ε' and ε'' in the X- and Ku-band region, for the studied composites. PLA-based composites exhibited relatively low ε'' values, suggesting limited dielectric losses across the investigated frequency range [25]. The most noticeable differences among the samples were found in the real component, ε', which reflects their ability to store electromagnetic energy. The systems containing IL presented the highest ε' values, indicating a stronger dielectric response in this frequency range compared to the composite without ILs. This behavior may be related to the influence of ILs on the dispersion of nanofillers and on the interfacial polarization processes, even though ε'' remained at relatively low levels.

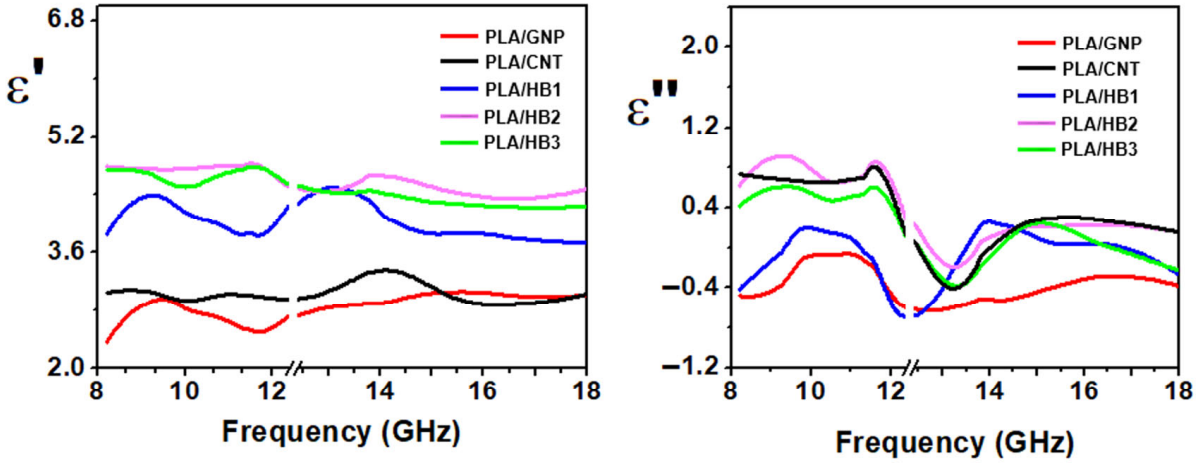


Figure 8. Real part (ε') and imaginary part (ε'') of the complex permittivity in the X- and Ku-band frequency range for the PLA nanocomposites.

RL values can be calculated from measured data of permittivity and permeability, which was used to estimated from the impedance matching theory, according to Equations (3) and (4) [66,67]:

$$Z_{in} = \sqrt{\frac{\mu_r}{\varepsilon_r}}\, tanh\left| j\left(\frac{2\pi\, fd}{c}\right)\sqrt{\mu_r \varepsilon_r}\right| \quad (3)$$

$$RL\ (dB) = 20log\left|\frac{Z_{in} - Z_0}{Z_{in} + Z_0}\right| \quad (4)$$

where ε_r and μ_r are the complex permittivity and permeability, respectively, f is the frequency, c is the velocity of light, and d is the sample thickness. From the Z_{in} values, the RL was calculated according to Equation (4), where Z_0 is the impedance of the air. The calculated RL plots of the composites containing the hybrid filler at different thickness are shown in Figure S2 of Supporting Information. PLA/HB1 (without IL) displays the best RL (−14 dB) with the thickness corresponding to 2.5 mm, whereas the best response for the system containing IL was achieved with 3 mm. In fact, PLA/HB2 (with IL1) and PLA/HB3 (with IL2) exhibited minimum RL values of −23.9 dB and −34 dB, respectively, and a larger EAB, as summarized in Table 4. The improved EM attenuation observed for the composites containing the GNP/CNT hybrids functionalized with ILs may be attributed to a better dispersion of the filler that causes an increase in interfaces to interact with the EM wave. This feature resulted in an increase in interfacial polarization. Moreover, the polarity of the ILs also contributes to the increasing in dipole polarization, thus improving the absorbing properties.

Table 4. Calculated RL and EAB of the PLA containing hybrid fillers as a function of sample thickness.

Sample	GNP (wt%)	CNT (wt%)	IL (wt%)	Thickness (mm)	RL (dB)	Frequency (GHz)	EAB (GHz)
PLA/HB1	2.5	0.5	-	2.5	−14	13.3	1.8
				3.0	−9.3	12.9	-
PLA/HB2	2.5	0.5	0.5 of IL1	2.5	−21.2	12.7	2.5
				3.0	−23.9	13.8	2.3
PLA/HB3	2.5	0.5	0.5 of IL2	2.5	−11.3	12.8	0.7
				3.0	−34.0	12.8	2.1

Figure S3 compares the measured RL obtained directly from the S_{11} scattering parameter of the VNA and calculated RL obtained from Equations (3) and (4). For the PLA/HB1, the measured RL was lower than the calculated one at the X-band, and almost coincides in the Ku-band. However, the systems containing HB2 and HB3 (with IL1 and IL2) displayed measured and calculated RL at quite similar frequency but the calculated values were lower than the measured one. The discrepancy between the measured and calculated RL values is attributed to the theoretical assumption based on isotropic materials [68], which is not the case of PLA containing HB fillers.

Table 5 compares the microwave absorbing properties of some PLA-based composites with the results obtained in the present study. The RL values achieved here are noteworthy when considering the low filler loading (3 wt%) and the relatively small thickness (3 mm). Lower RL values than those reported in this work have typically been obtained only by using high loadings of hybrid fillers involving magnetite and ferrites, often combined with a 3D-printing fabrication process. In another study, Cordeiro et al. [50] reported a RL value of −40.4 dB using 5.5 wt% GNP in a PLA/liquid isoprene rubber (LIR) blend matrix. In that case, the heterogeneous polymer blend likely enhanced the dispersion of filler, thus favoring the interactions between the GNP particles and the incident EM wave.

Table 5. Comparative analysis of microwave absorbing properties of some PLA-based composites reported in the literature.

Matrix	Filler		Thickness	RL	f	EAB	Procedure	Ref
	Type	Content (%)	(mm)	(dB)	(GHz)	(GHz)		
PLA/PHBV	CNT/GNP	1:3	2.6	−29	10.7	2.78	melt mixing	[47]
PLA	GNP	6	6.7	−12.3	6	0.46	melt mixing	[46]
PLA/PHBV	CNT	1	3.2	−16	11	2.9	melt mixing	[69]
PLA	GNP/Fe_3O_4	25.6	2.65	−50		4.16	extrusion/3D printing	[70]
PLA	GNP	8	1.5	−19.2	13	2.9	solution/compression	[13]
PLA	GNP/Mn-Zn ferrite	4:20	2.5	−24.3	15	5.12	extrusion/3D printing	[71]
PLA	FeSiAl/Fe_3O_4/GNP	30:4	5.3	−50.2		3.52	extrusion/3D printing	[72]
PLA/EVA	CNT	0.9	1.5	−26	13.6	1.3	Melt mixing	[73]
PLA	GNP/Fe_2O_3	5:5	2.5	−30	11.7	3.5	extrusion/3D printing	[74]
PLA/LIR	GNP	5.5	2.0	−40.4	8.4	2.18	melt mixing	[50]
PLA/EVA	GNP/$bmimBF_4$	5	3	−31	14.8	3.7	melt mixing	[40]
PLA	Fe_3O_4@GNP	10	3	−30	13.3	1.81	melt mixing	[75]
PLA	GNP/CNT/IL2	2.5/0.5	3	−34	12.8	2.1	solution/melt mixing	this work

3.5. Microwave Absorbing Properties of Multilayer Structure

Multilayered structures represent a highly promising strategy for enhancing EM wave attenuation and achieving broadband absorption, primarily through improved impedance matching and multiple internal reflection [29,67,76,77]. By selecting a first layer with optimized surface impedance, incident EM waves can readily penetrate the absorber with minimal reflection and undergo successive reflections and scattering events within the stacked layers, thereby promoting effective energy dissipation [50]. In this work, the composites were assembled by stacking three layers, each 1 mm thick, on a metal backing plate acting as a perfect reflector. The total thickness of 3 mm was selected due to the outstanding

RL and EAB responses estimated with this thickness. It is important to emphasize that this configuration has no practical applications in situations without metal as the backed plate. The two configurations were investigated, using either PLA/CNT (0.5 wt%) or PLA GNP (3.0 wt%) as the first (or matching) layer. These materials were chosen due to their relatively low conductivity, which facilitates EM wave penetration. The hybrid filler served as the middle layer, while the final layer in contact with the metal plate was again either PLA/CNT (0.5 wt%) or PLA GNP (3.0 wt%). Figure 9 presents the measured RL versus frequency for the three-layer structure composites with two arrangements, and the corresponding EM parameters are also summarized in Table 6. All multilayered systems exhibited minimum RL values below −10 dB, corresponding to more than 90% EM wave attenuation, and achieved significantly broader effective absorption bandwidths (EAB) than their monolayer counterpart, as shown in Figure 7. When PLA/GNP was used as the matching layer, the strongest EM wave attenuation occurred in the Ku-band frequency range, with the PLA/HB1 composite (PLA/GNP/CNT (2.5:0.5 wt%) as the middle layer reaching a minimum RL of −29.6 dB. Systems incorporating HB2 and HB3 as the middle layer offered a wider EAB. Conversely, when PLA/CNT served as the first layer, enhanced attenuation was observed in the X-band, with the CNT/HB3/GNP three-layer arrangement providing the optimal combination of minimum RL and larger EAB. These improvements arise from the abundant interfacial regions within and between the layers, which promote multiple reflection, and scattering enhancing energy dissipation via interfacial and dielectric losses. Although both PLA/CNT and PLA/GNP function effectively as matching layers due to their low conductivity, the reduced CNT content in the PLA/CNT composite also contributed to a better impedance matchings, thus improving wave penetration. Additionally, the RL performance of the multilayer structures depends on the interaction between filler dispersion, dielectric response (ε' and ε''), and impedance matching imposed by the intermediate layer. In this context, the improved RL observed for CNT/HB3/GNP, in contrast to the reduced performance of GNP/HB2/CNT, indicates that HB3 promotes more effective impedance matching, leading to deeper reflection loss minima, whereas HB2 favors higher effective absorption bandwidth (EAB) due to a more balanced dielectric response, although with less optimal matching in this specific configuration.

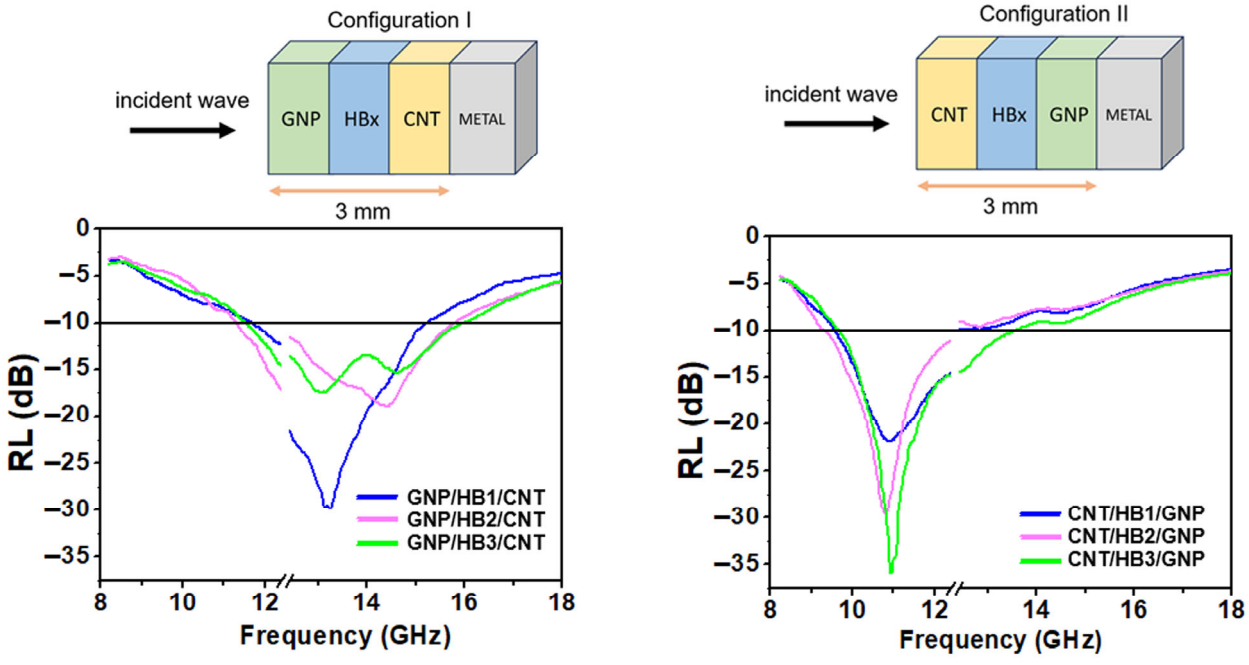


Figure 9. Measured RL in the X- and Ku-band for the PLA-based three-layered structure composites using the metal-backed configuration, as a function of the hybrid filler in the middle layer.

Table 6. RL and EAB of PLA-based three-layered structure composites as a function of the hybrid filler in the middle layer.

Structure Code	RL (dB)	f (GHz)	EAB (GHz)
GNP/HB1/CNT	−29.6	13.2	3.53
GNP/HB2/CNT	−18.7	14.4	4.50
GNP/HB3/CNT	−17.3	13.05	4.35
CNT/HB1/GNP	−21.7	10.9	2.80
CNT/HB2/GNP	−29.4	10.8	3.10
CNT/HB3/GNP	−35.6	10.9	3.80

Overall, these results confirm the critical role of multilayered architectures, together with appropriate layer sequencing, in developing lightweight, broadband microwave absorbers for stealth and electromagnetic shielding applications.

4. Conclusions

This work investigated the effect of alkyl-phosphonium and triphenyl-phosphonium-based ionic liquids (ILs) as noncovalent dispersing agents for hybrid GNP/CNT fillers on the dielectric, dynamic-mechanical, and microwave absorbing properties of PLA composites. The composites were produced via solution-assisted sonication followed by melt mixing and compression molding. Incorporation of GNP/CNT with PLA matrix at a weight ratio of 2.5:0.5 wt% led to a pronounced increase in melt viscosity and AC electrical conductivity compared with binary PLA/CNT and PLA/GNP systems. This behavior is attributed to the synergistic interaction between the two fillers, promoting the formation of a hybrid percolated network within the PLA matrix.

Noncovalent functionalization of the hybrid filler with 0.5 wt% ILs decreased the conductivity of the system, consistent with the formation of an insulating layer on the carbonaceous surfaces that disrupts conductive pathways in some extent. Concurrently, a significant increase in dielectric permittivity was observed, which is associated with enhanced interfacial polarization (MWS effect) arising from the increased number of internal interfaces able to block the mobile charge carriers. This behavior was more pronounced with PLA/HB3 system, likely due to the higher polarity of the IL2 and its better compatibility with PLA, due to the presence of the carboxyl group in its structure. These results confirm the effectiveness of ILs in improving the filler dispersion.

Composite containing hybrid filler modified with 11-carboxyundecyl-triphenyl-phosphonium bromide IL (IL2) (PLA/HB3) exhibited increased storage modulus, indicating enhanced filler-matrix interactions promoted by the presence of carboxyl group in the IL structure.

In terms of microwave absorption, the systems containing IL (PLA/HB2 and PLA/HB3) showed the lowest RL with an optimal matching thickness of 3 mm. Also the larger EAB was observed in the Ku-band frequency range for both systems with ILs. Furthermore, a three-layer configuration with optimized layer sequencing significantly broadened the EAB. A minimum RL of −35.6 dB (corresponding to >99.9% of EM attenuation) and an EAB of 3.8 GHz were achieved using PLA/CNT as the front layer and the IL2-modified composite as the core layer. Overall, the incorporation of low loadings (3 wt%) of IL-modified hybrid carbo fillers into a PLA matrix enables the development of multifunctional, microwave absorbing bio-based composites with potential applications in "green" electronics and stealth related technologies. Moreover, the outstanding permittivity of the systems containing ILs also suggest their application in energy storage, devices.

Supplementary Materials: The following supporting information can be downloaded at: https://www.mdpi.com/article/10.3390/jcs10010050/s1, Figure S1: G′ and G″ plots against the frequency; Figure S2: Calculated RL plots of the composites containing the hybrid fillers at different thickness; Figure S3: Measured RL obtained directly from the S11 scattering parameter of the VNA analyser an calculated RL obtained from the Equations (3) and (4).

Author Contributions: Conceptualization, R.R.H.; methodology, A.S. and R.R.H.; validation, B.G.S. and R.R.H.; formal analysis, B.G.S.; investigation, A.S. and R.R.H.; resources, B.G.S.; writing—original draft preparation, R.R.H.; writing—review and editing, B.G.S.; supervision, B.G.S.; project administration, B.G.S.; funding acquisition, B.G.S. All authors have read and agreed to the published version of the manuscript.

Funding: This research was funded by Fundação de Amparo à Pesquisa do Estado do Rio de Janeiro—FAPERJ, grant number E-26/210757/2021 and E-26/203974/2024; and Conselho Nacional de Desenvolvimento Científico e Tecnológico—CNPq, grant number 408839/2022-8.

Data Availability Statement: The datasets generated during and/or analyzed during the current study are available from the corresponding author on reasonable request.

Conflicts of Interest: The authors declare no conflicts of interest.

References

1. Nagarajan, V.; Mohanty, A.K.; Misra, M. Perspective on polylactic acid (PLA) based sustainable materials for durable applications: Focus on toughness and heat resistance. *ACS Sustain. Chem. Eng.* **2016**, *4*, 2899–2916. [CrossRef]
2. Nampoothiri, K.M.; Nair, N.R.; John, R.P. An overview of the recent developments in polylactide (PLA) research. *Bioresour. Technol.* **2010**, *101*, 8493–8501. [CrossRef]
3. Muthuraj, R.; Manjusri, M.; Amar, K.M. Biodegradable compatibilized polymer blends for packaging applications: A literature review. *J. Appl. Polym. Sci.* **2018**, *135*, 45726. [CrossRef]
4. De Luca, S.; Milanese, D.; Gallichi-Nottiani, D.; Cavazza, A.; Sciancalepore, C. Poly(lactic acid) and Its Blends for Packaging Application: A Review. *Clean Technol.* **2023**, *5*, 1304–1343. [CrossRef]
5. da Silva Pens, C.J.; Klug, T.V.; Stoll, L.; Izidoro, F.; Flores, S.H.; de Oliveira Rios, A. Poly (lactic acid) and its improved properties by some modifications for food packaging applications: A review. *Food Packag. Shelf Life* **2024**, *41*, 101230. [CrossRef]
6. Tyler, B.; Gullotti, D.; Mangraviti, A.; Utsuki, T.; Brem, H. Polylactic acid (PLA) controlled delivery carriers for biomedical applications. *Adv. Drug Deliv. Rev.* **2016**, *107*, 163–175. [CrossRef] [PubMed]
7. Gonçalves, C.; Gonçalves, I.C.; Magalhães, F.D.; Pinto, A.M. Poly(lactic acid) Composites Containing Carbon-Based Nanomaterials: A Review. *Polymers* **2017**, *9*, 269. [CrossRef]
8. Bayer, I.S. Thermomechanical Properties of Polylactic Acid-Graphene Composites: A State-of-the-Art Review for Biomedical Applications. *Materials* **2017**, *10*, 748. [CrossRef]
9. Olhan, S.; Behera, B.K. Development of GNP nanofiller based textile structural composites for enhanced mechanical, thermal, and viscoelastic properties for automotive components. *Adv. Compos. Hybrid Mater.* **2024**, *7*, 75. [CrossRef]
10. Adekoya, G.J.; Ezika, A.C.; Adekoya, O.C.; Sadiku, E.R.; Hamam, Y.; Ray, S.S. Recent advancements in biomedical application of polylactic acid/graphene nanocomposites: An overview. *BMEMat* **2023**, *1*, 12042. [CrossRef]
11. Mobaraki, M.; Liu, M.; Masoud, A.-R.; Mills, D.K. Biomedical Applications of Blow-Spun Coatings, Mats, and Scaffolds—A Mini-Review. *J. Compos. Sci.* **2023**, *7*, 86. [CrossRef]
12. Liu, T.; Feng, H.; Zeng, W.; Jin, C.; Kuang, T. Facile Fabrication of Absorption-Dominated Biodegradable Poly(lactic acid)/Polycaprolactone/Multi-Walled Carbon Nanotube Foams towards Electromagnetic Interference Shielding. *J. Compos. Sci.* **2023**, *7*, 395. [CrossRef]
13. Wang, S.; Yang, W.; Li, X.; Hu, Z.; Wang, B.; Gong, N. Volume exclusion effect and ambient temperature induced ultrahigh electromagnetic wave absorption properties of polylactic acid (PLA)/graphene nano-platelets (GNPs) composites. *J. Appl. Polym. Sci.* **2024**, *141*, 55370. [CrossRef]
14. Cataldi, P.; Athanassiou, A.; Bayer, I.S. Graphene Nanoplatelets-Based Advanced Materials and Recent Progress in Sustainable Applications. *Appl. Sci.* **2018**, *8*, 1438. [CrossRef]
15. Kausar, A.; Ahmad, I.; Zhao, T.; Aldaghri, O.; Ibnaouf, K.H.; Eisa, M.H.; Lam, T.D. Graphene Nanocomposites for Electromagnetic Interference Shielding—Trends and Advancements. *J. Compos. Sci.* **2023**, *7*, 384. [CrossRef]
16. Peixoto, T.; Nunes, J.; Lopes, M.A.; Marinho, E.; Proença, M.F.; Lopes, P.E.; Paiva, M.C. Poly(lactic acid) composites with few layer graphene produced by noncovalent chemistry. *Polym. Compos.* **2022**, *43*, 8409–8425. [CrossRef]

17. Dehnou, K.H.; Norouzi, G.S.; Majidipour, M. A review: Studying the effect of graphene nanoparticles on mechanical, physical and thermal properties of polylactic acid polymer. *RSC Adv.* **2023**, *13*, 3976–4006. [CrossRef] [PubMed]
18. Gonçalves, C.; Pinto, A.; Machado, A.V.; Moreira, J.; Gonçalves, I.C.; Magalhães, F. Biocompatible reinforcement of poly(lactic acid) with graphene nanoplatelets. *Polym. Compos.* **2018**, *39*, E308–E320. [CrossRef]
19. Silva, M.; Gomes, C.; Pinho, I.; Gonçalves, H.; Vale, A.C.; Covas, J.A.; Alves, N.M.; Paiva, M.C. Poly(lactic acid)/grafite nanoplatelet nanocomposite filaments for ligament scaffolds. *Nanomaterials* **2021**, *11*, 2796. [CrossRef]
20. Atif, M.; Qiang, T.; Yasar, M.; Zafar, J.; Tahira, K.; Han, W.; Sadia, B.; Faris, R.; Alanazi, A.K. Development and characterization of graphene/PLA composites: Balancing mechanical, thermal, and optical properties for packaging applications. *Macromol. Res.* **2025**, *33*, 1683–1696. [CrossRef]
21. Siddiqui, V.U.; Sapuan, S.M.; Ariffin, M.K.A.M.; Hassan, M.R. Mechanical, thermal, viscoelastic, and electrical performance evaluation of graphene nanoplatelets/polylactic acid (PLA) (GNP/PLA) nanocomposites. *Int. J. Precis. Eng. Manuf.* **2026**, *27*, 277–295. [CrossRef]
22. Kallambadi Sadashivappa, P.; Venkatachalam, R.; Pothu, R.; Boddula, R.; Banerjee, P.; Naik, R.; Radwan, A.B.; Al-Qahtani, N. Progressive Review of Functional Nanomaterials-Based Polymer Nanocomposites for Efficient EMI Shielding. *J. Compos. Sci.* **2023**, *7*, 77. [CrossRef]
23. Jalali, A.; Kheradmandkeysomi, M.; Buahom, P.; Gupta, T.; Habibpour, S.; Omranpour, H.; Park, C.B. Engineering lightweight poly (lactic acid) graphene nanoribbon nanocomposites for sustainable and stretchable electronics: Achieving exceptional electrical conductivity and electromagnetic interference shielding with enhanced thermal conductivity. *Carbon* **2024**, *226*, 109. [CrossRef]
24. Bregman, A.; Michielssen, E.; Taub, A. Comparison of Experimental and Modeled EMI Shielding Properties of Periodic Porous xGNP/PLA Composites. *Polymers* **2019**, *11*, 1233. [CrossRef]
25. Kashi, S.; Gupta, R.K.; Baum, T.; Kao, N.; Bhattacharya, S.N. Dielectric properties and electromagnetic interference shielding effectiveness of graphene-based biodegradable nanocomposites. *Mater. Des.* **2016**, *109*, 68. [CrossRef]
26. Kashi, S.; Gupta, R.K.; Baum, T.; Kao, N.; Bhattacharya, S.N. Morphology, electromagnetic properties and electromagnetic interference shielding performance of poly lactide/graphene nanoplatelet nanocomposites. *Mater. Des.* **2016**, *96*, 119. [CrossRef]
27. Al-Saleh, M.H.; Al-Sharman, M.M. Influence of graphene nanoplatelets geometrical characteristics on the properties of polylactic acid composites. *Diam. Relat. Mater.* **2022**, *126*, 165052. [CrossRef]
28. Al-Saleh, M.H.; Al-Sharman, M.M. Influence of carbon nanofiller geometry on EMI shielding and electrical percolation behaviors of polymer composites. *Synth. Met.* **2023**, *294*, 117314. [CrossRef]
29. Silva, J.M.F.; Indrusiak, T.; Barra, G.M.O.; Letichevsky, S.; Silva, A.A.; Soares, B.G. Hybrid carbonaceous filler as promising additives for EMI SE of PVDF-based composites: Comparison between monolayered and multilayered structures. *FlatChem* **2024**, *43*, 100603. [CrossRef]
30. Wang, J.; Li, H.; Wang, Z.; Xin, D.; Luo, J.; Bai, S.; Zhou, H. Improved electromagnetic interference shielding properties of poly (vinylidene fluoride) composites based on carbon nanotubes and graphene nanoplatelets. *Polym. Compos.* **2022**, *43*, 6966. [CrossRef]
31. Luo, X.; Yang, G.; Schubert, D.W. Electrically conductive polymer composite containing hybrid graphene nanoplatelets and carbon nanotubes: Synergistic effect and tunable conductivity anisotropy. *Adv. Compos. Hybrid Mater.* **2022**, *5*, 250. [CrossRef]
32. Shukla, M.K.; Sharma, K. Effect of functionalized graphene/CNT ratio on the synergetic enhancement of mechanical and thermal properties of epoxy hybrid composite. *Mater. Res. Express* **2019**, *6*, 085318. [CrossRef]
33. Shi, S.; Peng, Z.; Jing, J.; Yang, L.; Chen, Y. 3D printing of delicately controllable cellular nanocomposites based on polylactic acid incorporating graphene/carbon nanotube hybrids for efficient electromagnetic interference shielding. *ACS Sustain. Chem. Eng.* **2020**, *8*, 7962–7972. [CrossRef]
34. Lv, Q.; Tao, X.; Shi, S.; Li, Y.; Chen, N. From materials to components: 3D-printed architected honeycombs toward high-performance and tunable electromagnetic interference shielding. *Compos. Part B Eng.* **2022**, *230*, 109500. [CrossRef]
35. Tunckol, M.; Durand, J.; Serp, P. Carbon nanomaterial- ionic liquid hybrids. *Carbon* **2012**, *50*, 4303–4334. [CrossRef]
36. da Silva, J.P.S.; Soares, B.G.; Livi, S.; Barra, G.M.O. Phosphonium–based ionic liquid as dispersing agent for MWCNT in melt-mixing polystyrene blends: Rheology, electrical properties and EMI shielding effectiveness. *Mater. Chem. Phys.* **2017**, *189*, 16. [CrossRef]
37. dos Santos, S.C.; Soares, B.G.; Pereira, E.C.L.; Indrusiak, T.; Silva, A.A. Impact of phosphonium-based ionic liquids-modified carbon nanotube on the microwave absorbing properties and crystallization behavior of poly (vinylidene fluoride) composites. *Mater. Chem. Phys.* **2022**, *280*, 125853. [CrossRef]
38. Pereira, E.C.L.; Soares, B.G.; Silva, A.A.; da Silva, J.M.F.; Barra, G.M.O.; Livi, S. Conductive heterogeneous blend composites of PP/PA12 filled with ionic liquids treated-CNT. *Polym. Testing* **2019**, *74*, 187–195. [CrossRef]
39. Soares, B.G.; Cordeiro, E.; Maia, J.; Pereira, E.C.L.; Silva, A.A. The effect of the noncovalent functionalization of CNT by ionic liquid on electrical conductivity and electromagnetic interference shielding effectiveness of semi-biodegradable polypropylene/poly (lactic acid) composites. *Polym. Compos.* **2020**, *41*, 82–93. [CrossRef]

40. Gabino, A.; Soares, B.G.; da Silva, E.F. Ionic liquid-aided liquid phase exfoliation of graphene and improved electric and electromagnetic properties of PLA/EVA/graphene composites. *FlatChem* **2025**, *52*, 100893. [CrossRef]
41. Xu, P.; Huang, B.; Tang, R.; Wang, Z.; Tu, J.; Ding, Y. Improved mechanical and EMI shielding properties of PLA/PCL composites by controlling distribution of PIL-modified CNTs. *Adv. Comp. Hybrid Mater.* **2022**, *5*, 991–1002. [CrossRef]
42. Gupta, S.; Tai, N.H. Carbon materials and their composites for electromagnetic interference shielding effectiveness in X-band. *Carbon* **2019**, *152*, 159–187. [CrossRef]
43. Soares, B.G.; Barra, G.M.O.; Indrusiak, T. Conducting Polymeric Composites Based on Intrinsically Conducting Polymers as Electromagnetic Interference Shielding/Microwave Absorbing Materials—A Review. *J. Compos. Sci.* **2021**, *5*, 173. [CrossRef]
44. Jayalakshmi, C.G.; Inamdar, A.; Anand, A.; Kandasubramanian, B. Polymer matrix composites as broadband radar absorbing structures for stealth aircrafts. *J. Appl. Polym. Sci.* **2019**, *136*, 47241. [CrossRef]
45. Ahmad, H.; Tariq, A.; Shehzad, A.; Faheem, M.S.; Shafiq, M.; Rashid, I.A.; Khaliq, Z. Stealth technology: Methods and composite materials—A review. *Polym. Compos.* **2019**, *40*, 4457–4472. [CrossRef]
46. Kashi, S.; Gupta, R.K.; Bhattacharya, S.N.; Varley, R.J. Experimental and simulation study of effect of thickness on performance of (butylene adipate-co-terephthalate) and poly lactide nanocomposites incorporated with graphene as stand-alone electromagnetic interference shielding and metal-backed microwave absorbers. *Compos. Sci. Technol.* **2020**, *195*, 108186. [CrossRef]
47. dos Anjos, E.G.R.; Brazil, T.R.; de Melo Morgado, G.F.; Antonelli, E.; Rezende, M.C.; Pessan, L.A.; Passador, F.R. Renewable PLA/PHBV blend-based graphene nanoplatelets and carbon nanotube hybrid nanocomposites for electromagnetic and electric-related applications. *ACS Appl. Electron. Mater.* **2023**, *5*, 6165–6177. [CrossRef]
48. Wu, Y.; Wang, Z.; Liu, X.; Shen, X.; Zheng, Q.; Xue, Q.; Kim, J.K. Ultralight graphene foam/conductive polymer composites for exceptional electromagnetic interference shielding. *ACS Appl. Mater. Interfaces* **2017**, *9*, 9059–9069. [CrossRef]
49. Panwar, R.; Lee, J.R. Recent advances in thin and broadband layered microwave absorbing and shielding structures for commercial and defense applications. *Funct. Compos. Struct.* **2019**, *1*, 032001. [CrossRef]
50. Cordeiro, E.P.; Gabino, A.D.A.; Soares, B.G. Conducting PLA/Liquid Isoprene Rubber/Graphene Nanoplatelets for Green Electromagnetic Absorbing Packaging Materials. *J. Appl. Polym. Sci.* **2025**, *143*, e70013. [CrossRef]
51. Wang, P.; Song, J.; Liu, J.; Gao, S.; Tian, H.; Xiao, B.; Zhou, Y.; Zhu, L.; Song, T.; Li, Z.; et al. Super-tough poly(lactide)/ethylene-methyl acrylate-glycidyl methacrylate random terpolymer blends via efficient catalytic interfacial crosslinking of environmentally friendly carboxyl-functionalized ionic liquids. *J. Polym. Environ.* **2024**, *32*, 3992–4004. [CrossRef]
52. Wang, P.; Zhou, Y.; Hu, X.; Wang, F.; Chen, J.; Xu, P.; Ding, Y. Improved mechanical and dielectric properties of PLA/EMA-GMA nanocomposites based on ionic liquids and MWCNTs. *Compos. Sci. Technol.* **2020**, *200*, 108347. [CrossRef]
53. Marins, J.A.; Soares, B.G.; Silva, A.A.; Hurtado, M.G.; Livi, S. Electrorheological and dielectric behavior of new ionic liquid/silica systems. *J. Colloid Interface Sci.* **2013**, *405*, 64–70. [CrossRef] [PubMed]
54. Rostami, A.; Nazockdast, H.; Karimi, M. Graphene induced microstructural changes of PLA/MWCNT biodegradable nanocomposites: Rheological, morphological, thermal and electrical properties. *RSC Adv.* **2016**, *6*, 49747–49759. [CrossRef]
55. Trinkle, S.; Friedrich, C. Van Gurp-Palmen-plot: A way to characterize polydispersity of linear polymers. *Rheol. Acta* **2001**, *40*, 322–328. [CrossRef]
56. Kashi, S.; Gupta, R.K.; Baum, T.; Kao, N.; Bhattacharya, S.N. Phase transition and anomalous rheological behaviour of polylactide/graphene nanocomposites. *Compos. Part B Eng.* **2018**, *135*, 25–34. [CrossRef]
57. Yeh, J.T.; Tsou, C.H.; Huang, C.Y.; Chen, K.N.; Wu, C.S.; Chai, W.L. Compatible and crystallization properties of poly (lactic acid)/poly (butylene adipate-*co*-terephthalate) blends. *J. Appl. Polym. Sci.* **2010**, *116*, 680–687. [CrossRef]
58. Wu, B.; Wu, Y.; Zhang, M.; Guo, H.; Liu, T.; Lin, G.; Kuang, T. Enhanced Mechanical and Multifunctional Properties of GNPs/CNTs Hybridized PLA Nanocomposites by Implementing Dual-Processing of Pickering Emulsion-Melt Blending Methods. *Macromol. Mater. Eng.* **2025**, *310*, 2400306. [CrossRef]
59. Carelo, J.C.; Soares, B.G.; Schmitz, D.P.; Henriques, R.R.; Silva, A.A.; Barra, G.M.O.; Barthem, V.M.T.S.; Livi, S. Magnetic Ionic Liquid: A Multifunctional Platform for the Design of Hybrid Graphene/Carbon Nanotube Networks as Electromagnetic Wave-Absorbing Materials. *Molecules* **2025**, *30*, 985. [CrossRef]
60. Zhao, B.; Zhao, C.; Li, R.; Hamidinejad, S.M.; Park, C.B. Flexible, ultrathin, and high-efficiency electromagnetic shielding properties of poly (vinylidene fluoride)/carbon composite films. *ACS Appl. Mater. Interfaces* **2017**, *9*, 20873–20884. [CrossRef]
61. Xu, P.; Gui, H.; Wang, X.; Hu, Y.; Ding, Y. Improved dielectric properties of nanocomposites based on polyvinylidene fluoride and ionic liquid-functionalized graphene. *Compos. Sci. Technol.* **2015**, *117*, 282–288. [CrossRef]
62. Xu, P.; Gui, H.; Hu, Y.; Bahader, A.; Ding, Y. Dielectric properties of polypropylene-based nanocomposites with ionic liquid-functionalized multiwalled carbon nanotubes. *J. Electron. Mater.* **2014**, *43*, 2754–2758. [CrossRef]
63. Sharma, M.; Sharma, S.; Abraham, J.; Thomas, S.; Madras, G.; Bose, S. Flexible EMI shielding materials derived by melt blending PVDF and ionic liquid modified MWNTs. *Mater. Res. Express* **2014**, *1*, 035003. [CrossRef]
64. Wang, D.; Bao, Y.; Zha, J.W.; Zhao, J.; Dang, Z.M.; Hu, G.H. Improved dielectric properties of nanocomposites based on poly (vinylidene fluoride) and poly (vinyl alcohol)-functionalized graphene. *ACS Appl. Mater. Interfaces* **2012**, *4*, 6273. [CrossRef]

65. Dang, Z.M.; Yuan, J.K.; Zha, J.W.; Zhou, T.; Li, S.T.; Hu, G.H. Fundamentals, processes and applications of high-permittivity polymer–matrix composites. *Prog. Mater. Sci.* **2012**, *57*, 660. [CrossRef]
66. Meng, F.; Wang, H.; Huang, F.; Guo, Y.; Wang, Z.; Hui, D.; Zhou, Z. Graphene-based microwave absorbing composites: A review and prospective. *Compos. Part B Eng.* **2018**, *137*, 260–277. [CrossRef]
67. Indrusiak, T.; Pereira, I.M.; Heitmann, A.P.; Silva, J.G.; Denadai, Â.M.L.; Soares, B.G. Epoxy/Ferrite Nanocomposites as Microwave Absorber Materials: Effect of Multilayered Structure. *J. Mater. Sci. Mater. Electron.* **2020**, *31*, 13118–13130. [CrossRef]
68. Pozar, D.M. *Microwave Engineering*; John Wiley & Sons, Inc.: Hoboken, NJ, USA, 2005; pp. 57–64.
69. Silva, A.P.B.; Montagna, L.S.; Passador, F.R.; Rezende, M.C.; Lemes, A.P. Biodegradable nanocomposites based on PLA/PHBV blend reinforced with carbon nanotubes with potential for electrical and electromagnetic applications. *Express Polym. Lett.* **2021**, *15*, 987–1003. [CrossRef]
70. Yan, T.; Ye, X.; He, E.; Gao, Q.; Wang, Y.; Ye, Y.; Wu, H. GR-Fe_3O_4/PLA 3D printing composite materials with excellent microwave absorption properties. *J. Alloys Compd.* **2024**, *972*, 172799. [CrossRef]
71. Ye, X.; Gao, Q.; Yang, P.; Yang, C.; He, E.; Ye, Y.; Wu, H. Mechanical and microwave absorbing properties of graphene-Mn-Zn ferrite/polylactic acid composites formed by fused deposition modeling. *J. Mater. Sci.* **2023**, *58*, 2525–2538. [CrossRef]
72. He, E.; Yan, T.; Ye, X.; Gao, Q.; Yang, C.; Yang, P.; Ye, Y.; Wu, H. Preparation of FeSiAl-Fe3O4 reinforced graphene/polylactic acid composites and their microwave absorption properties. *J. Mater. Sci.* **2023**, *58*, 11647–11665. [CrossRef]
73. Pereira, E.C.L.; Fernandes, M.E.; Santos, J.; Calheiros, L.F.; Silva, A.A.; Soares, B.G. Broadband microwave absorbing materials for green electronics based on poly(lactic acid)/ethylene-vinyl acetate copolymer blends loaded with carbon nanotube. *J. Appl. Polym. Sci.* **2022**, *139*, e52510. [CrossRef]
74. Amudhu, L.B.T.; Samsingh, R.V.; Florence, S.E.; Prakash, C.A. Electromagnetic wave absorption and mechanical properties of 3D-printed PLA composites reinforced with graphene and iron (III) oxide for X-band absorbers. *J. Mater. Sci. Mater. Electron.* **2024**, *35*, 1273. [CrossRef]
75. Henriques, R.R.; Souto, L.F.C.; Silva, A.A.; Soares, B.G. Bio-based PLA composites loaded with Fe_3O_4/graphene nanoplatelet hybrids for improved microwave absorbing properties. *Mater. Sci. Eng. B* **2025**, *314*, 117994. [CrossRef]
76. Danlée, Y.; Bailly, C.; Huynen, I. Thin and flexible multilayer polymer composite structures for effective control of microwave electromagnetic absorption. *Compos. Sci. Technol.* **2014**, *100*, 182–188. [CrossRef]
77. Guo, Z.; Ren, P.; Fu, B.; Ren, F.; Jin, Y.; Sun, Z. Multi-layered graphene-Fe_3O_4/poly (vinylidene fluoride) hybrid composite films for high-efficient electromagnetic shielding. *Polym. Test.* **2020**, *89*, 106652. [CrossRef]

Disclaimer/Publisher's Note: The statements, opinions and data contained in all publications are solely those of the individual author(s) and contributor(s) and not of MDPI and/or the editor(s). MDPI and/or the editor(s) disclaim responsibility for any injury to people or property resulting from any ideas, methods, instructions or products referred to in the content.